

ISOCAM DEEP SURVEYS UNVEILING STAR FORMATION IN THE MID-INFRARED

D. Elbaz¹, H. Aussel¹, C.J. Césarsky¹, F.X. Désert², D. Fadda¹, A. Franceschini³, J.L. Puget², J.L. Starck¹¹Service d'Astrophysique, CEA/DSM/DAPNIA Saclay, Orme des Merisiers, 91191 Gif-sur-Yvette Cédex, France
fax +33.1.69.08.65.77, e-mail elbaz@cea.fr²Institut d'Astrophysique Spatiale, Bât 121, Université Paris XI, F-91405 Orsay Cédex, France³Osservatorio Astronomico di Padova, Italy

ABSTRACT

Before having exhausted the helium in its tank on April 8, 1998, the Infrared Space Observatory had time to perform several complementary surveys at various depths and areas within selected regions of the sky. We present the results of some of the surveys done with the mid-infrared camera, ISOCAM, on-board ISO, and more specifically those surveys which were performed using the broad-band filter LW3 (12-18 μm).

We show that mid-infrared allows to discriminate starburst and post-starburst galaxies among galaxies which present similar optical-UV morphological and colour signatures. Furthermore, the strong evolution found in the surveys indicates that more star formation is hidden in the infrared at higher redshifts.

Key words: cosmological surveys; mid-infrared; galaxy evolution.

1. INTRODUCTION

The so-called 'Madau plot' (Madau *et al.* 1996) which follows the rate of star formation per unit comoving volume in the universe as a function of the redshift presents the advantage of being global enough to give an indication of the past history of star formation as a whole, avoiding the difficulties encountered when trying to separate the respective role of individual galaxy types (Sp/Pec/E, hierarchical galaxy formation vs individual collapse, duration of the bursts). However, based on optical-UV information only it is now clear that this plot only sets a lower limit to the total star formation history of the universe (see below).

This plot also addresses the question of the heavy element content of the universe as a way to normalize the past history of star formation in the universe. Assuming that there was little margin left for more star formation than already found from optical-UV light one could see the lower limits given by Madau *et al.* 1996 as if they were firm constraints. Since

then Lyman-break galaxies (also called UV drop-out galaxies) found by Steidel *et al.* (1996) appeared to be strongly affected by dust obscuration. Pettini *et al.* (1997) estimated that about two thirds of the emission due to star formation taking place in these galaxies is radiated in the infrared as indicated by the slope of their rest-frame UV spectral energy distribution (see also Meurer *et al.* 1997, for the strong UV absorption at high redshifts). The metal content of the local universe presents enough uncertainties to leave margin for hidden star formation, especially at high redshifts where time flows faster per unit redshift. Among those uncertainties, we shall quote the lack of galactic globular clusters with more than solar metallicity which would be required to calibrate the metallicity of metal rich stellar populations found in elliptical galaxies; the presence of at least as much metals in the intra-cluster medium of galaxy clusters than in the galaxies themselves (Arnaud *et al.* 1992, Mushotzky & Loewenstein 1997), with an overabundance of α -elements which may indicate a biased IMF in the early stages of star formation in ellipticals (Elbaz *et al.* 1995a); the still uncertain precise value and universality of the IMF. There is clearly space for a factor 2-4 in the heavy elements content of the local universe which implies a large freedom in the star formation history of the distant universe where time is so short.

Although these indirect arguments already favour dust-enshrouded star formation with respect to optical-UV estimates in Lyman-break galaxies (Pettini *et al.* 97), the correction for dust obscuration remains controversial and direct observations in the infrared are critical at this stage. The obvious way to go for it is the far infrared (FIR) since the spectral energy distribution (SED) of dusty star forming regions peaks around 60 μm . IRAS was not sensitive enough to probe the universe above $z \simeq 0.2$, except for some exceptionnally bright objects such as 10214+4724 (Rowan-Robinson *et al.* 1991). FIRAS on-board COBE detected a diffuse far-infrared to sub-mm background (Puget *et al.* 1996, Guiderdoni *et al.* 1997, Fixsen *et al.* 1998). The origin of this Cosmic InfraRed Background (CIRB) remains controversial and could either be due to a local population of galaxies ($z \simeq 1$) as proposed by Fall, Charlot & Pei (1996) or by a population of galaxies distributed over a wider redshift range as suggested by Puget *et al.* (1996 and this conference, and Lagache

et al. 1998). The recent detection of a population of distant dusty galaxies at 450 and 850 μm with the sub-mm array camera SCUBA on the JCMT (Smail, Ivison & Blain 1997, Blain *et al.* 1998, Cimatti *et al.* 1998, Barger *et al.* 1998, Hughes *et al.* 1998) tends to favour a shift of the peak of the star formation rate per unit comoving volume towards larger redshifts. These observations would favour the distant galaxy population option to explain the CIRB. However, finding counterparts with spectroscopic redshift to these SCUBA galaxies will be the next step to answer this question. There will also still remain an uncertainty on the FIR part of the SED since sub-mm wavelengths only probe the right side of the peak, even at $z=3$ where the peak of the SED is redshifted to 240 μm . Reliable quantitative estimates of the SFR will only become available when the rest-frame FIR part of the SED will be sampled. For this purpose, ISOPHOT on-board ISO, is not sensitive enough, although tantalizing results are already obtained at 175 μm (Kawara *et al.* 1998, Lagache *et al.* 1998, Puget *et al.* 1998). The satellite FIRST will certainly play a major role in this respect.

However, one can already see that hidden star formation plays a major role. Although the mid-infrared range is less directly correlated with star formation than larger wavelengths, we will show that with a 1000 times better sensitivity and 60 times better spatial resolution than IRAS, ISOCAM mid-infrared deep surveys confirm that most star formation is hidden by dust and that this effect increases with redshift ($z < 1.5$).

2. ORIGIN OF THE MID-INFRARED EMISSION AND ITS LINK WITH STAR FORMATION

The rest frame mid-IR emission of galaxies can be divided into three components (Puget & Léger 1989, Désert *et al.* 1990):

- **UIBs:** the large Unidentified Infrared Bands (UIBs), detected at 6.2, 7.7, 8.6, 11.3 and 12.7 μm as well as their underlying continuum, dominate the mid-IR emission below 12 μm (see figure 1). The carriers of these UIBs contain Polycyclic Aromatic Hydrocarbons (PAHs, Léger & Puget 1984, Puget & Léger 1989). The fact that in the wavelength range where the mid-infrared emission is dominated by UIBs globally scales with the intensity of the radiation field with only small changes in the spectrum shape is a strong indication that the carriers of the UIBs are transiently heated by the absorption of individual photons (Boulanger 1998). The mid-infrared emission of galaxies does increase with the star formation rate though saturating for strong radiation fields (Boselli *et al.* 1998).
- **Warm dust ($T > 150$ K):** continuum at $\lambda > 10$ μm from Very Small Grains (VSGs) of dust (Désert *et al.* 1990).
- **Forbidden lines of ionized gas:** NeII (12.8 μm), NeIII (15.6 μm), SIV (10.5 μm), ArII (7 μm). These lines are good indicators of the star formation activity, particularly the NeIII/NeII ratio,

when using the low resolution spectro-imagery mode of ISOCAM for nearby galaxies, but their contribution to large bands such as those used for the deep surveys is negligible.

All three components affect the 12-18 μm ISOCAM filter (LW3) due to K-correction for galaxies between redshifts 0 and 1.5. Indeed, the LW3 band includes emission from very small grains for low redshifts and becomes more and more contaminated by UIBs with increasing redshift.

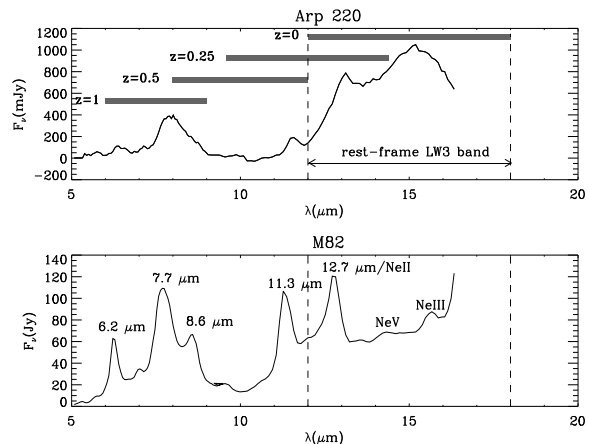


Figure 1. SEDs from ISOCAM Circular Variable Filter. Upper plot: M82 (Tran 1998), UIBs nearly absent, high ratio of the 12-18 μm over the 5-8.5 μm band. Lower plot: Arp 220 (Charmandaris *et al.* 1998), strong UIB features and low ratio of the 12-18 μm over the 5-8.5 μm band.

The Far Infrared (FIR) flux is usually assumed to be correlated to the SFR once the cirrus emission is removed (see Scoville & Soifer 1991, Kennicutt 1998). The MIR emission is also a strong indicator of star formation, but the derivation of a star formation rate exclusively from the MIR flux is tricky: while many active star forming galaxies exhibit comparable infrared SEDs, some are very different. The mid-IR over far-IR ratio can vary between less than 1 % and a few times 10 %. This results directly from the complex underlying physics of the mid-infrared emission which differs from the FIR one. For example, let us compare Arp 220 and M82 (see table 1 and figure 1):

Both galaxies emit approximately the same 15 μm flux relative to visible light (respectively 3 , for Arp 220, and 4, for M82, times more energy is radiated at 15 μm than at 0.55 μm). The contribution of the far infrared part of the spectrum relative to the MIR is substantially different: the ratio of the FIR to MIR light is 10 times larger for Arp 220 than for M82. This difference of an order of magnitude in FIR luminosity would imply one order of magnitude difference in star formation rate (using the formula given by Scoville & Soifer 1991 or Kennicutt 1998). Hence, the mid-IR flux cannot be considered as a direct measure of the star formation rate, assuming a linear correlation between 15 and 60 μm fluxes. However, Arp 220 is an extreme case and most galaxies behave more like M82 than Arp 220, so that the uncertainty is probably closer to 5 than to 10.

Table 1. Comparison of M82 & Arp 220: two template nearby starburst galaxies ($H_0=75 \text{ km.s}^{-1} \text{ Mpc}^{-1}$, distances corrected for the Virgo infall: $d(\text{M82})=3 \text{ Mpc}$, $d(\text{Arp220})=73 \text{ Mpc}$). See Genzel *et al.* 1998 for a discussion showing that the emission of Arp 220 is dominated by its starburst activity and not its central AGN.

Waveband	Arp 220	M82	$\frac{\text{Arp220}}{\text{M82}}$
Visible (L_V^{Tot})	$2.6 \times 10^9 L_\odot$	$4.3 \times 10^8 L_\odot$	6
LLW3 (12-18 μm)	$7.5 \times 10^9 L_\odot$	$1.6 \times 10^9 L_\odot$	4.7
LFIR (8-1000 μm)	$1.3 \times 10^{12} L_\odot$	$2.5 \times 10^{10} L_\odot$	52
$LLW3/L_V^{\text{Tot}}$	2.9	3.7	1.3
$LFIR/L_V^{\text{Tot}}$	500	58	8.6
$LFIR/LLW3$	173	16	11

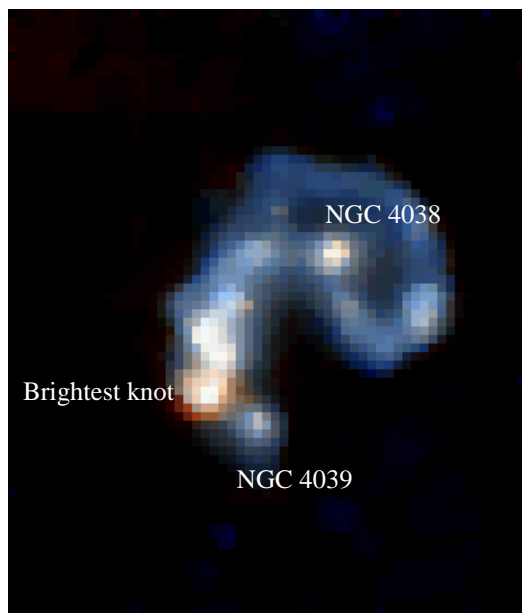


Figure 2. mid-infrared image of the Antennae galaxies. The bright spot lies in the overlapping region of the two interacting galaxies NGC 4038/4039, while the optical-UV emission peaks at the position of the two galaxy nuclei (Vigroux *et al.* 1996)

If the link between mid-IR fluxes and star formation is not simple and implies the need for a multi-wavelength approach to reach reliable quantitative estimates of the star formation rate, the case of the Antennae galaxy is sufficiently explicit by itself to prove that hidden star formation can be unveiled through its mid-IR emission (Mirabel *et al.* 1998). ISOCAM mid-infrared imaging indeed revealed a bright spot (see figure 2, from Vigroux *et al.* 1996) which emits alone 15 % of the total mid-IR emission, within the overlapping region of the two interacting galaxies NGC 4038/4039 (Mirabel *et al.* 1998). This spot is clearly optically obscured and most of the optical emission arises from the two galactic nuclei.

The spectral energy distribution at the position of this spot presents two emission lines, NeII and NeIII, which do not appear as clearly on the brightest optical spots corresponding to the two galaxy nuclei, with a ratio of NeIII over NeII close to one, hence in-

dicating the presence of massive young stars (figure 3, Mirabel *et al.* 1998).

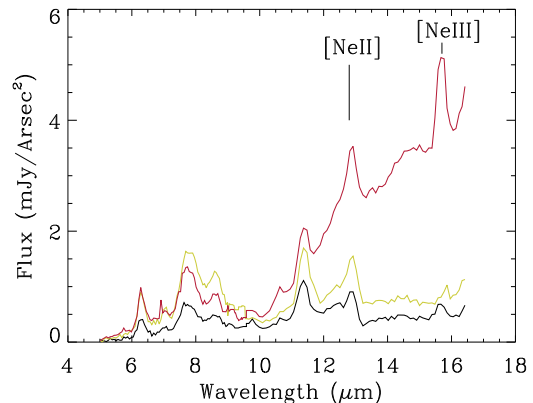


Figure 3. CVF spectra of 3 regions in the Antennae galaxy (NGC 4038/4039): the 2 bottom plots correspond to the 2 galaxy nuclei, while the upper curve is associated to the brightest 15 μm spot in the overlapping region of the 2 galaxies.

3. ISOCAM DEEP SURVEYS

Several Deep Surveys have been performed using ISOCAM on-board ISO ranging from very large and shallow ones (ELAIS, P.I. M. Rowan-Robinson) to smaller and deeper ones (figure 4).

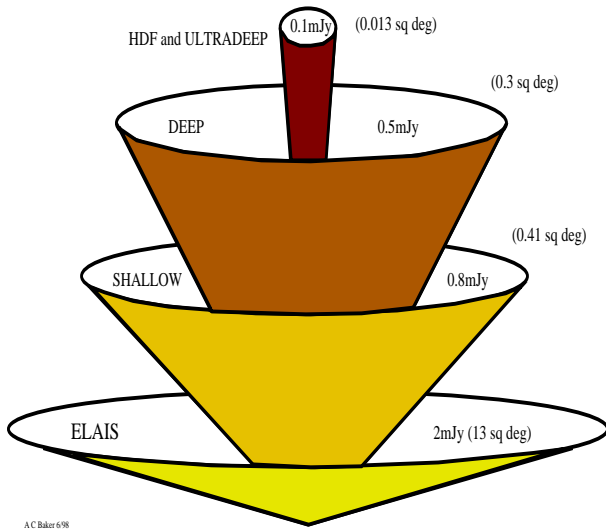
As shown by the number counts plot (section 3.3.), all these surveys are complementary since they explore the behaviour of galaxies in the mid-IR over nearly 4 orders of magnitude in the Log N-Log S plot. All surveys have been performed in regions of the sky relatively clean of cirrus and zodiacal emission: the Lockman Hole and Marano Field regions, but also the Hubble Deep Field region. The main limitation of these surveys comes from the presence of cosmic ray impacts on the detector for the detection and completeness limits (see below) and from the transient behaviour due to the very low temperature of the detectors for the photometry accuracy.

3.1. Data reduction

ISOCAM data are subject to standard gaussian noise (photon and readout noises) and to errors associated with the flat-fielding and dark current subtraction. But the main limitation of ISOCAM deep surveys comes from its thick and cold pixels:

- because they are very thick, ISOCAM pixel detectors are very sensitive to cosmic ray impacts (4.5 pixels receive a glitch per second). The behaviour of these glitches can be divided into three families:
 - "normal glitches": the more common ones, which correspond to electrons and last only

ISOCAM Extragalactic Surveys



A.C. Baker 6/98
(c) CEA 1998 - tous droits réservés

Figure 4. ISOCAM extragalactic surveys (from A. Baker).

one or two readouts only. They are easily removed by using a median filtering (the combination of several scales for the median allows the best correction).

- "faders": these glitches as well as the following ones are probably associated with protons and alpha particles. They induce positive peaks in the detector response, which can last several readouts. Since ISOCAM is best used in the raster mode, a real source will look like these glitches, i.e. a positive response over the number of readouts spent on a given position of the sky.
- "dippers": some glitches are followed by a trough extending over more than one hundred readouts.

We have developed a tool based on the multi-resolution wavelet transform developed by Starck *et al.* which finds and removes the "faders" and "dippers". This tool, named PRETI, for Pattern REcognition Technique for Isocam data, looks for the signal above the n -sigma level at different frequencies or scales in the wavelet transform of the original signal. Being extended these glitches will be detected over several successive scales as typical patterns. Using their wavelet coefficients, one can subtract a smooth function corresponding to the glitch in the raw signal and use the output signal in the co-addition of all pixels of the raster that fall on the same sky position (see figure 5).

- ISOCAM pixels are cold, so that electrons move very slowly within them and therefore induce a transient behaviour: a pixel will take several hundred readouts to stabilize when moving from the background to the position of a source on the sky and inversely. Because of time limitation, one is therefore limited to non stabilized signals which results in an uncertainty on the photometry. This uncertainty is strongly reduced by the partial correction of the transient behaviour and

by the use of simulations to define a statistical distribution of measured fluxes for any given input flux. The final uncertainty on ISOCAM deep survey fluxes is on the order of 20 %.

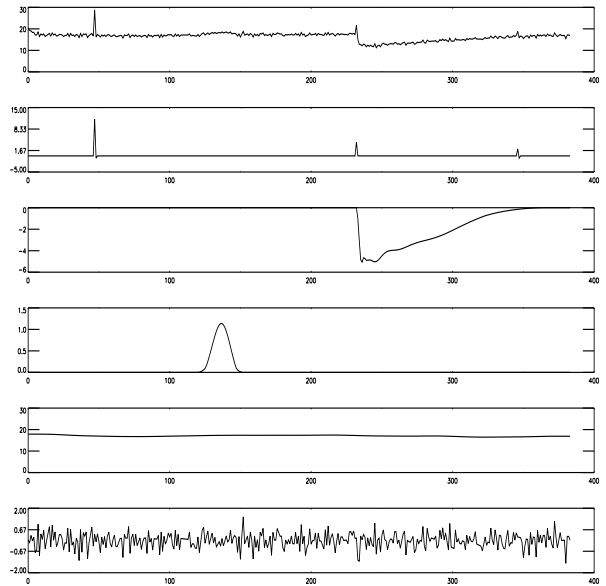


Figure 5. These plots show the decomposition of the signal measured by a given pixel of the camera as a function of the number of readouts, in different frequencies or wavelet coefficients. From top to bottom: the first plot presents the typical time behaviour of a given ISOCAM pixel. One can see from left to right: a "normal" glitch, a faint source which extends over $\simeq 20$ readouts, a "dipper", with long trough, and a "normal" glitch again, at the end of the trough. The second plot, shows the high frequency signal corresponding to the "normal" portion of the glitches. The third plot shows the reconstructed signal of the dipper's trough, after combining the information from several frequencies or scales of the signal. The fourth plot presents a gaussian at the position of the source with the extent of the source (we do not extract the signal at this frequency since it contains sources, but this plot is only intended to indicate the position of the source). The fifth plot shows the low frequency part of the signal, i.e. its baseline. The last plot presents the residual of the signal after extraction of the glitches and baseline. The source was subtracted to show only the gaussian noise residual, due to photon and readout noise. Very faint sources are not visible on the time history of a given pixel and only appear after co-adding the residual of all pixels which pointed towards the same sky direction on a final raster map.

In order to facilitate the separation of sources from cosmic ray impacts, ISOCAM surveys were performed using the raster mode with redundancy (number of different pixels falling successively on a given sky position) ranging from 2 for the shallowest survey (ELAIS) to 88 for the deepest surveys (Marano Field Ultra-Deep survey; 64 for the HDF field).

3.2. Simulations

We performed simulations in order to quantify the sensitivity limit (minimum detected flux, below the

completeness limit), the completeness limit (flux above which all sources are detected) and the photometric accuracy. These simulations were performed with real datasets (in order to simulate realistic glitches) in which we introduced fake sources including the PSF and their modeled transient: a long staring observation (more than 500 readouts) was used to simulate a raster observation. Real sources would extend over the whole observation and would be removed as a low frequency component of the signal while in a raster observation sources only remain during the number of readouts spent on a given position of the sky. Figure 6 shows as an example a simulation of what an HDF-like ISOCAM deep survey would look like at $15 \mu\text{m}$ if the source distribution followed the strongly evolving model developed by Franceschini *et al.* (1991). The next section will present the real dataset to be compared with these simulations.

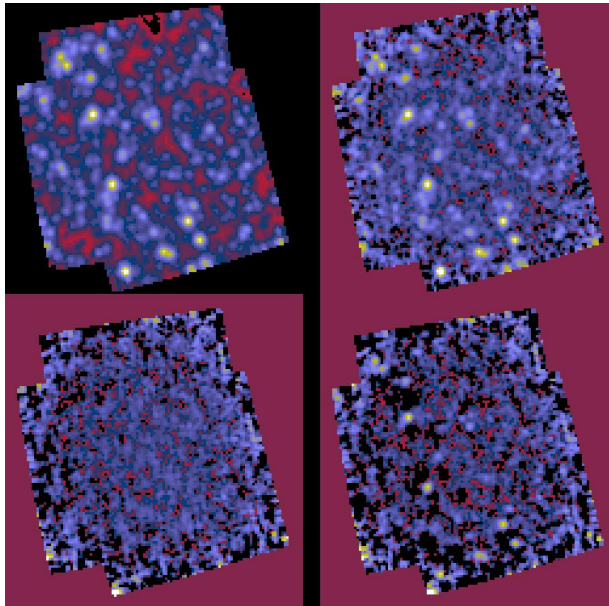


Figure 6. simulated ISOCAM-HDF: from upper-left to bottom-right. The first image shows the distribution of sources expected from the model with strong evolution of Franceschini *et al.* 1994, where the number of galaxies per unit luminosity per unit redshift is given by: $N(L,z)=N(L,z=0)\times\exp(\kappa\tau)$ where κ is the evolution parameter ($\kappa=3$) and τ is the lookback time $= (t_0 - t)/t_0$. Fluxes are ranging from $0.1 \mu\text{Jy}$ to 1 mJy . Only the PSF is included and there is no noise associated with this “ideal” image. In the second image, the ISOCAM gaussian noise resulting from the readout and photon noise was added to the previous image. The last image presents the final image that ISOCAM would see including the noise introduced by cosmic ray impacts, shown in the third image.

Finally, we also developed two independent data analysis techniques at Saclay (PRETI, Starck 1998) and Orsay (Tripple beam-switch technique, see Désert *et al.* 1998), in order to test the confidentiality level of the results. We find an agreement at the 20 % level corresponding to the photometric error of both techniques, an astrometric error close to the pixel size and compatible source lists. In the case of the Hubble Deep Field, we compared our results to the new results of the team of M.Rowan-Robinson, which differ from their first analysis in the photom-

etry at $15 \mu\text{m}$, because the techniques on each side were improved with time (see Aussel *et al.* 1998).

3.3. RESULTS

Source detection was performed on the output images of PRETI (see figure 7 & figure 8 for the ISOCAM HDF and Lockman Hole Deep Survey fields) using a spatial multi-scale wavelet transform. Hence multi-scale transforms were performed at two stages of the data analysis: first, on the temporal history of the detector pixels in order to remove glitches, then on the final co-added image for the source detection. The photometry of the Tripple Beam-Switch technique from Désert *et al.* 1998 and PRETI are consistent at the 20 % level.

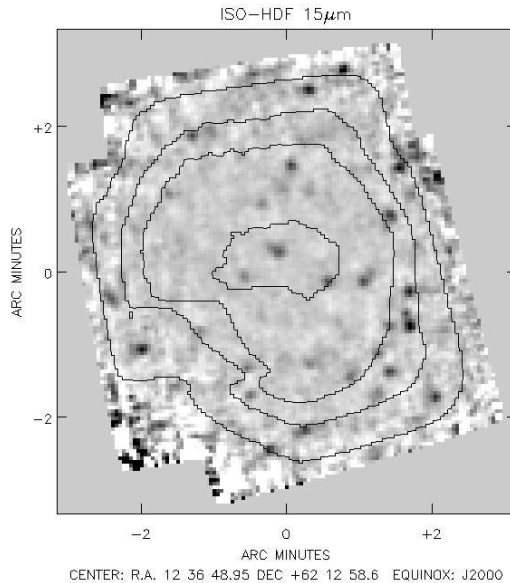


Figure 7. ISOCAM $15 \mu\text{m}$ HDF image from Aussel *et al.* (1998). Compare this image to the simulation shown in the previous image. The excess of detections found in the real image reflects the high evolution parameter needed to reproduce the number counts below ($\kappa=6$ instead of 3).

Several hundreds of simulated images were done in order to estimate from a Monte Carlo statistical approach the limits of our results in terms of photometric accuracy and completeness. We have included this information in the Log N-Log S curve (figure 9): error bars on the fluxes and the flux range where completeness is achieved result directly from the Monte Carlo simulations.

The number counts are presented here in the two classical forms: the log N-log S (figure 9), gives the number of objects which flux is higher than a given flux limit $S(\text{mJy})$, and the differential counts normalized to euclidean (figure 10). No evolution would give a slope of $3/2$ in the Log N-log S in a euclidean space (2.5 in the differential counts, by derivation): at larger distances, d , the number of objects increases as a function of the volume, i.e. in d^3 , but decreases due to dimming in d^{-2} . In a relativistic universe the slope of the no evolution curve is even lower than that

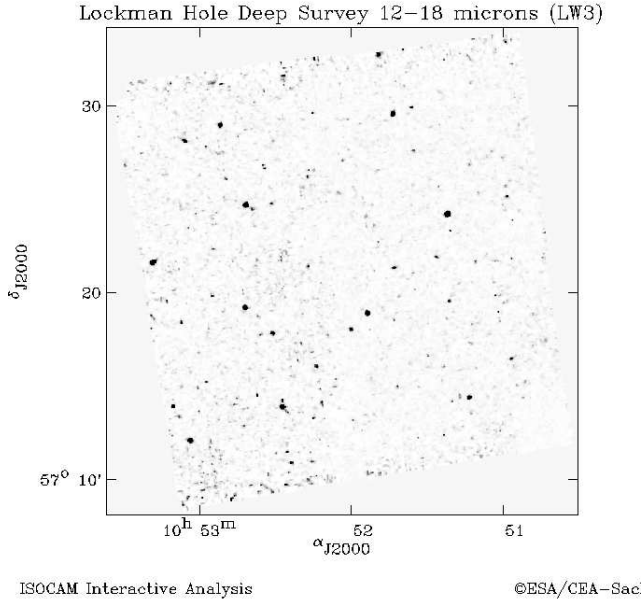


Figure 8. ISOCAM 15 μm Lockman Hole Deep Survey image from Elbaz *et al.* 1998.

as shown by the no-evolution curve from Franceschini (1998) overplotted on figure 9.

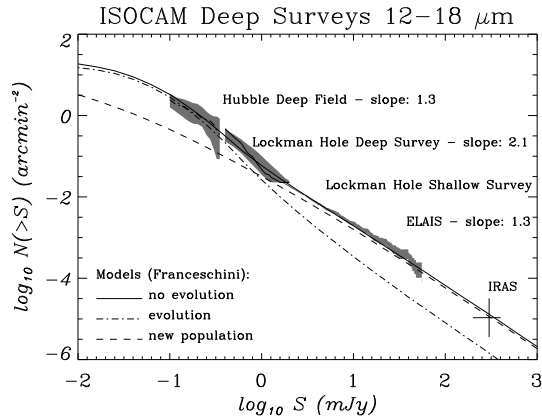


Figure 9. $\log N(S)$ - $\log S$: number of objects, N , detected above a given flux level, S (μJy), with ISOCAM in the 15 μm broad band filter LW3. The data are consistent although they come from 5 different origins, from high fluxes to low fluxes one finds: ISOCAM-HDF (from Aussel *et al.* 1998), Lockman Hole deep survey (Elbaz *et al.* 1998), Lockman Hole shallow survey (Elbaz *et al.* 98), ELAIS (ELAIS consortium, P.I. M.Rowan-Robinson, Oliver *et al.* 1998), IRAS 12 μm (Spinoglio *et al.* 1995). Dashed line: no evolution, normalized to IRAS and including PAH features. Dashed-dotted line: strongly evolving population in $N(L,z)=N(L,z=0)\times\exp(\kappa\tau)$ with $\kappa=6$. Plain line: sum of the no evolution + strongly evolving population. The strongly evolving population becomes dominant below 1 mJy

3.4. Interpretation

For the first time, we present number counts over 4 orders of magnitude ranging from 100 μJy , in the

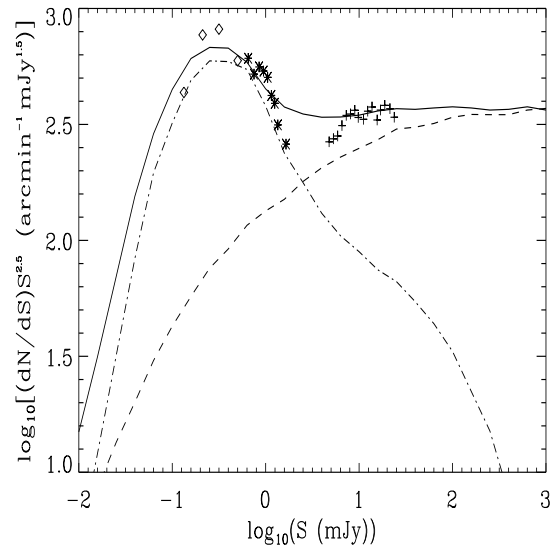


Figure 10. euclidean normalized differential counts: ISOCAM-HDF (diamonds), Lockman Hole deep survey (stars), ELAIS (crosses). The models are the same as in the $\log N$ - $\log S$ plot.

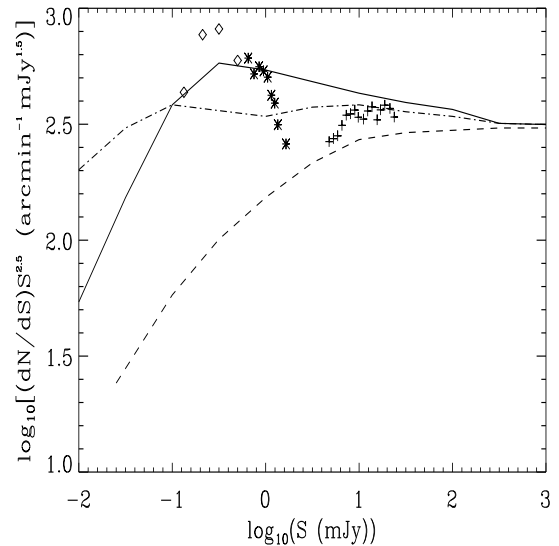


Figure 11. euclidean normalized differential counts: same as above. Models of Xu *et al.* (1998) normalized to . Plain line: pure luminosity evolution, $\rho \propto (1+z)^4$. Dashed-dotted line: pure density evolution, $\rho \propto (1+z)^3$. Dashed line: no evolution.

ISOCAM-HDF (Aussel *et al.* 1998), to 50 mJy, in the ELAIS fields (ELAIS consortium, P.I. M.Rowan-Robinson, Oliver *et al.* 1998) and up to 300 mJy, including the IRAS 12 μm counts. It can be seen on both the $\log N$ - $\log S$ (figure 9) and the differential counts (figure 10) that above the 1 mJy level, no strong departure from no evolution is indicated while below this flux level, a rapid rise appears (clearly seen on the differential counts plot). Such a trend cannot be reproduced either by the PAHs features,

which effect on the K-correction is too weak, or by a continuous evolution of the “standard” form for all galaxies. We tried three such laws:

1. pure luminosity evolution as described in Franceschini *et al.* (1991): $N(L,z)=N(L,0) \times \exp(\kappa\tau)$ where κ is the evolution parameter and $\tau = (t_0-t)/t_0$ is the lookback time. No value of κ allows to fit the data, except if we consider a separate population of objects which becomes dominant below the 1 mJy level, i.e. above $z \simeq 0.4$.
2. pure luminosity evolution used by Pearson & Rowan-Robinson (1996) to fit the IRAS 60 μm number counts, proportional to $(1+z)^3$ and calculated by Xu *et al.* (1998) at 15 μm (figure 11).
3. the pure density evolution, in $(1+z)^4$, from Xu *et al.* (1998, figure 11).

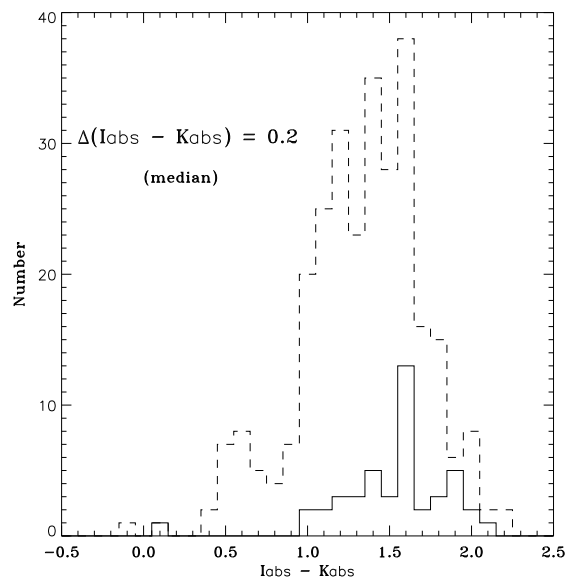


Figure 12. Histogram of the I-K rest-frame colours of all HDF+Flanking fields galaxies (dashed line) and HDF+Flanking fields galaxies detected at 15 μm above 100 μJy . The rest-frame colours were calculated using the K-correction from Coleman *et al.* 1980. The difference in the median colours is only 0.2 dex.

Extreme evolution needs to be added to the no-evolution curve, which could be associated with a galaxy population dominating the counts below 1 mJy, i.e. above $z=0.4$ (in this model). The evolution parameter, κ , required for this “population” is $\kappa=6$, while it was 3, in the original model with strong evolution of Franceschini *et al.* (1991). This rapid increase of the number counts below 1 mJy, corresponds to a high flux density in the mid-IR going towards faint fluxes. Integrating the number counts over the whole flux range one finds that about $2 \times 10^{-9} \text{ W.m}^{-2}.\text{sr}^{-1}$ is emitted at 15 μm and $3 \times 10^{-9} \text{ W.m}^{-2}.\text{sr}^{-1}$ when extrapolating the counts assuming no further increase in the slope. This corresponds to 30-45 % of the cosmic background seen with the HST in the I-band ($7 \times 10^{-9} \text{ W.m}^{-2}.\text{sr}^{-1}$). Locally about one third of the energy is radiated in

the infrared (Soifer & Neugebauer 1991) and mainly in the FIR since the FIR over MIR ratio is typically 3 for normal galaxies and stronger than 10 for starbursting galaxies. The cosmic infrared background is therefore larger than the optical background when integrating over a larger redshift range than IRAS, which implies that going towards higher redshifts:

- dust obscuration is stronger at higher redshift.
- a few bright infrared objects make most of the cosmic background, since the few detections at 15 μm in the HDF produce more integrated light than the large number of optically detected galaxies.

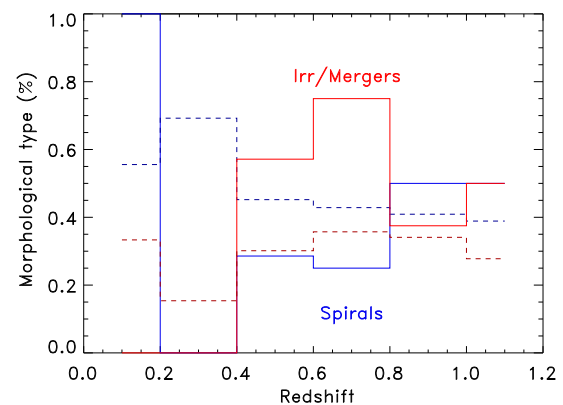


Figure 13. Fraction of Peculiar versus Spiral galaxies in the HDF+Flanking fields for galaxies detected at 15 μm (plain lines) and all galaxies (dashed lines). Above $z \simeq 0.4$, peculiar galaxies dominate the distribution of galaxies detected with ISOCAM while optically selected galaxies are mainly spirals. This population of peculiar galaxies may produce the rapid evolution below the 1 mJy level found in the 15 μm number counts.

This result agrees with those obtained with SCUBA (see references above) and with the CIRB estimates (see Puget *et al.*, these proceedings). Additional conclusions can be reached only after identification of the sources, and multi-wavelength and redshift measurements. We are currently gathering such data for the sources in the Lockman Hole. In the HDF (Elbaz *et al.* 1998) and in one of the CFRS fields, surveyed with ISOCAM by Flores *et al.* (1998), such data are available. We summarize some of the main conclusions obtained from this source by source comparison over $\simeq 60$ sources within the HDF+flanking fields with redshifts in the range 0.4-1.3:

- at $z 0.5$, peculiar, mergers and post-starburst galaxies are much more frequent in the ISO base than in the optical base (Flores *et al.* 1998, Elbaz *et al.* 1998, see figure 13). It is likely that the additional population required to account for the number counts is composed of such galaxies.
- Flores *et al.* (1998) attempt to fit the multi-wavelength data over 10 sources for which radio data are available. In this way, they estimate that the universal star formation at $z \simeq 1$ is enhanced by a factor 2.3 with respect to previously estimated UV fluxes.

Using available data on the HDF, we find that galaxies detected above 100 μJy (completeness limit reached in the HDF, Aussel *et al.* 1998) do not show any clear signature in their optical colours (see figure 12, Elbaz *et al.* 1998). The I-K colour of ISO-CAM detected galaxies is only 0.2 dex redder than all HDF galaxies.

3.5. CONCLUSION

We showed that even with very sensitive telescopes like the HST, optical observations need to be combined with infrared imaging in order to select the major events of star formation in the universe. The sensitivity required for the NGST to detect all HDF optical galaxies, i.e. 2×10^6 galaxies per square degree, at 15 μm would be about 0.02 μJy if the slope flattens as shown by the model on figure 9 and 0.3 μJy if a moderate evolution with a slope close to 1.3 continues below the 100 μJy level. For a large fraction of these galaxies, the NGST would resolve the regions of star formation in actively star forming galaxies and change our view on galaxy evolution without suffering from dust obscuration.

REFERENCES

- Arnaud, M., Rothenflug, R., Boulade, O., Vigroux, L., Vangioni-Flam, E 1992, A&A 254, 49
- Aussel, H., Cesarsky, C., Elbaz, D., Starck, J.L. 1998, to appear in A&A
- Barger, A.J. *et al.*, submitted to Nature, astro-ph/9806317
- Blain, A.W., Smail, I., Ivison, R.J., Kneib, J.P. 1998, submitted to MNRAS, astro-ph/9806062
- Boselli, A. *et al.* 1998, A&A 335, 53
- Boulanger, F. 1998, *Star Formation with the Infrared Space Observatory*, 24-26 June 1997, Lisbon, Portugal, edited by Joao Yun and Rene Liseau, Publisher: ASP, as volume 132 of ASP Conference Series. p. 15.
- Charmandaris, V. *et al.* 1998, in preparation
- Cimatti, A., Andreani, P., Rottgering, H., Tilanus, R. 1998, Nature 392, 895
- Coleman, G.D., Wu, C.C., Weedman, D.W. 1980, ApJ Suppl.Ser. 43, 393
- Désert, F.-X., Boulanger, F., Puget, J.-L. 1990, A&A 237, 215
- Désert, F.-X., *et al.* 1998, to appear in A&A
- Elbaz, D., Arnaud, M., Vangioni-Flam, E. 1995, A&A 303, 345
- Elbaz, D., *et al.* 1998, in preparation
- Fall, S.M., Charlot, S., Pei, Y.C. 1996, ApJ, L43
- Fixsen, D. J., Dwek, E., Mather, J. C., Bennett, C. L., Shafer, R. A. 1998, ApJ, in press
- Flores, H., F. Hammer, F.X. Désert, C. Césarsky, D. Crampton, A. Omont, T. Thuan, S. Eales, O. Le Fèvre, S.J. Lilly 1998, to be submitted to ApJ
- Franceschini, A., Toffolatti, L., Mazzei, P., Danese, L., De Zotti, G. 1991, A&A Suppl.Ser. 89, 285
- Franceschini, A. 1998, in T.Thuan, G. Mamon, and J.T.T.Van (eds), *Extragalactic Astronomy in the Infrared*, Proceedings of the XVIIth Moriond Astrophysics Meeting, Ed. Frontière, p.509.
- Genzel, R. *et al.* 1998, ApJ 498, 579
- Guiderdoni, B., Bouchet, F.R., Puget, J.L., Lagache, G., Hivon, E. 1997, Nature 390, 257
- Hughes, D., *et al.* 1998, to appear in Nature, astro-ph/9806297
- Kawara, K., *et al.* 1998, A&A 336, L9
- Kennicutt, R.C. 1998, ApJ 498, 541
- Lagache, G. 1998, to be submitted
- Léger, A., Puget, J.L. 1984, A&A 137, L5
- Madau, P., Ferguson, H.C., Dickinson, M.E., Giavalisco, M., Steidel, C.C., Fruchter, A. 1996, MNRAS 283, 1388
- Meurer, G.R., Heckman, T.M., Lehnert, M.D., Leitherer, C., Lowenthal, J. 1997, AJ 114, 54
- Mirabel, I.F. *et al.* 1998, A&A 333, L1
- Moorwod A. F. M. *et al.* 1996, A&A 315, L109
- Mushotzky, R.F., Loewenstein, M. 1997, ApJ 481, L63
- Pettini, M., Steidel, C.C., Adelberger, K.L., Kellogg, M., Dickinson, M., Giavalisco, M. 1997, astro-ph/9708117
- Puget, J.-L., Léger, A. 1989, Ann.Rev.Ast.Ap. 27, 37
- Puget, J.-L. *et al.* 1996, A&A 308, L5
- Puget, J.-L. *et al.* 1998, these proceedings
- Scoville, N.Z., Soifer, B.T. 1991, in *Massive Stars in Starbursts*, ed. Leitherer, C., Walborn, N., Heckman, T., Norman, C., Cambridge Univ. Press, p.233
- Soifer, B.T., Neugebauer, G. 1991, AJ 101, 354
- Spinoglio, L., Malkan, M.A., Rush, B., Carrasco, L., Recillas-Cruz, E. 1995, ApJ 453, 616
- Starck, J.L., Aussel, H., Elbaz, D., Cesarsky, C. 1998, in T.Thuan, G. Mamon, and J.T.T.Van (eds), *Extragalactic Astronomy in the Infrared*, Proceedings of the XVIIth Moriond Astrophysics Meeting, Ed. Frontière, p.509.
- Steidel, C.C., Giavalisco, M., Pettini, M., Dickinson, M., Adelberger, K.L. 1996, ApJ 462, L17
- Rowan-Robinson, M. *et al.* 1991, Nature 351, 719
- Smail, I, Ivison, R.J., Blain, A.W. 1997, ApJ 490L, 5
- Tran, D. 1998, PHD thesis
- Vigroux, L., *et al.* 1996, A&A 315, L93